ICASE

DTIC
SELECTE
DEC 0 6 1995
F

A FAR-FIELD NON-REFLECTING
BOUNDARY CONDITION FOR
TWO-DIMENSIONAL WAKE FLOWS

Jeffrey S. Danowitz
Saul A. Abarbanel
Eli Turkel

National Aeronautics and
Space Administration
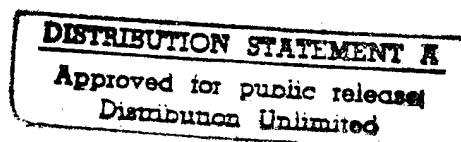
Langley Research Center
Hampton, Virginia 23681-0001

19951205 018

A FAR-FIELD NON-REFLECTING BOUNDARY CONDITION FOR TWO-DIMENSIONAL WAKE FLOWS

Jeffrey S. Danowitz   Saul A. Abarbanel*   Eli Turkel*

School of Mathematical Sciences
Sackler Faculty of Exact Sciences
Tel-Aviv University
Tel-Aviv, Israel

Abstract

Far-field boundary conditions for external flow problems have been developed based upon long-wave perturbations of linearized flow equations about a steady state far field solution. The boundary improves convergence to steady state in single-grid temporal integration schemes using both regular-time-stepping and local-time-stepping. The far-field boundary may be near the trailing edge of the body which significantly reduces the number of grid points, and therefore the computational time, in the numerical calculation. In addition the solution produced is smoother in the far-field than when using extrapolation conditions. The boundary condition maintains the convergence rate to steady state in schemes utilizing multigrid acceleration.

i

1 Introduction

Numerical solution schemes for nonlinear flow equations usually require the introduction of one or more artificial boundaries to be placed at some distance from a body around which (in external flows) the flow takes place. On these boundaries appropriate boundary conditions must be established that are not only physically correct, but that also comply with mathematical requirements as well. In, for example, subsonic flow regimes, it is well known that for hyperbolic flow equations (e.g. Euler Equations), one characteristic points back into the flow domain at outflow, and therefore one condition must be prescribed; the rest, called numerical boundary conditions, must be in some way consistent with the partial differential equations. This paper deals with the derivation of *outflow* (far-field) boundary conditions. These boundary conditions will be both temporally and spatially local.

The proper formulation of far-field conditions remains a vexing problem to date, and many authors have tried to tackle it in a variety of directions. It was once common in steady state calculations to set $p = p_\infty$, (p being pressure) and to, say, extrapolate all other quantities. Certainly this procedure is inappropriate for boundaries close to the body, and so alternate approaches are needed to be developed. At present, the Navier-Stokes solver, [9], uses extrapolation on all physical quantities in subsonic regimes (*note that in supersonic regimes, extrapolation of all variables is correct from a mathematical standpoint*) with great success. In fact, its authors claim that they have been unable to replace far-field extrapolation with another far-field condition and to achieve satisfactory steady state convergence [12].

It has become popular to place "non-reflecting" boundary conditions at outflow in subsonic flows. While it is true that generally one cannot develop local boundary conditions that give no reflections, one can consider conditions which to some degree are *better* than others. The notion of better in this case implies that (see [10])

- the reflections are decreased and steady state convergence is accelerated.

- the reflections will decrease as the position of the artificial boundary tends to infinity.

- as the incident wave is more normal to the artificial boundary, the reflections decrease.

In 1988 Abarbanel, Bayliss and Lustman (ABL) [1] developed a non-reflecting outflow boundary condition for viscous, compressible flows over a flat plate. Their idea was to linearize the Navier-Stokes equations around a far-field steady state solution

flow direction

Inflow

airfoil

l

wake region

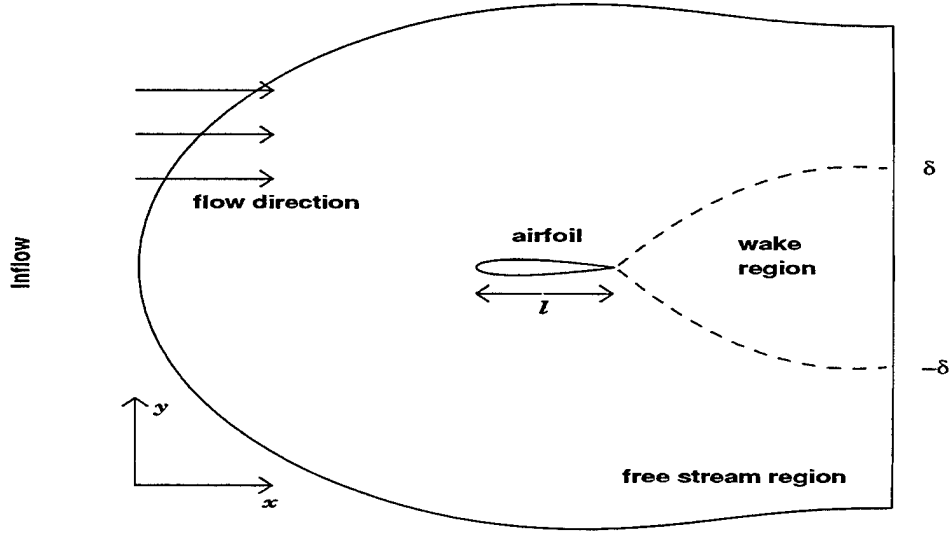δ

$-\delta$

y

x

free stream region

Figure 1: External flow topology for compressible viscous flows around NACA012

with an assumed u-velocity profile based upon an asymptotic approximation to the equations themselves. These linear perturbation equations were then assumed to take on a dispersive wave solution and the resulting set of equations (similar to the Orr-Sommerfeld system) described the asymptotic behaviour along the outflow boundary – the artificial boundary. Abarbanel, Bayliss and Lustman then assumed that the decay rate of the perturbations is mainly controlled by the iteration scheme's inability to dissipate long wave disturbances. So they expanded the system, including the wave frequency, around small wave numbers i.e. long waves. The resulting zeroth and first order eigensystems are solved for their eigenvalues. The eigenvalue of the zeroth order eigensystem physically corresponds to the decay rate of the long wave disturbances, and the eigenvalue of the first order eigensystem physically corresponds to the group velocity of these disturbances. The slowest decay rate is found, and it defines uniquely the group velocity. The details of the aforementioned strategy may be found in [1]. The outflow boundary condition derived from this takes on the form:

$$\frac{\partial p}{\partial t} + \alpha(p - p_\infty) = \beta \frac{\partial p}{\partial x} \qquad (1.1)$$

where $\alpha > 0$ is proportional to the decay rate of the disturbances, and $\beta < 0$ is their group velocity. This condition is very effective in the flat plate case.

This paper uses the ABL approach in developing a far-field nonreflecting boundary condition for two-dimensional wake flows. We consider two cases. The first being compressible viscous laminar flows around NACA0012, as illustrated in figure 1. In this case the compressible Navier-Stokes equations are numerically integrated using
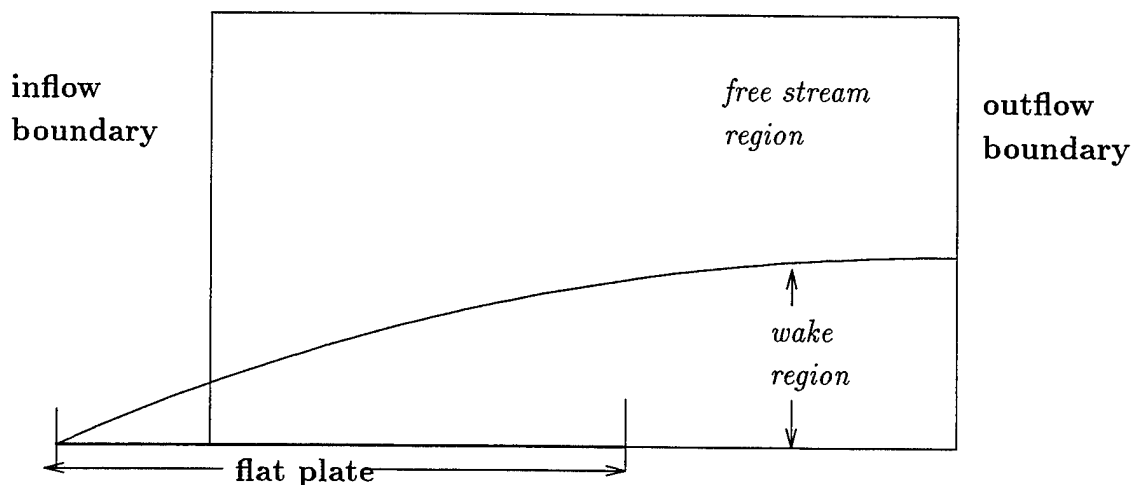
Figure 2: The flat plate topology for incompressible viscous boundary layer flows

a time consistent scheme. Multigrid acceleration has been used in this case as well.

The second case considered is incompressible viscous boundary layer flow over a finite flat plate as illustrated in figure 2. In this case the incompressible boundary layer equations are numerically integrated both time consistently and with local-time stepping.

The nonreflecting boundary condition has been developed accordingly for time-consistent cases with and without multigrid acceleration and for local-time-stepping cases without multigrid acceleration.

In §2 we outline the long wave asymptotic expansion procedure in the general compressible case and develop the appropriate eigensystem for this case. In §3 we consider the incompressible boundary layer case and extend the boundary condition to local-time-stepping schemes. Then in §4 we derive the non-reflecting boundary condition both with and without multigrid acceleration. In §5 we present numerical results beginning with the numerical procedure used to obtain the eigenvalues needed in building the boundary condition, and ending off with a general discussion of the results of all the numerical tests performed. In §6 we comment on the results.

2 Long Wave Asymptotic Expansions

The Navier-Stokes equations governing two-dimensional compressible flows may be written in the following form:

$$\begin{cases} continuity: & \rho_t + (\rho u)_x + (\rho v)_y = 0 \\ x - momentum: & \rho(u_t + u u_x + v u_y) + p_x = \mu(u_{xx} + u_{yy} + \frac{1}{3}(u_x + v_y)_x) \\ y - momentum: & \rho(v_t + u v_x + v v_y) + p_y = \mu(v_{xy} + v_{yy} + \frac{1}{3}(u_x + v_y)_y) \\ energy: & \rho c_v \frac{DT}{Dt} + p(u_x + v_y) = \nabla \cdot (\kappa \nabla T) + \Phi \end{cases} \qquad (2.1)$$

where ρ is the density, u and v are the x and y components of the velocity and p is the pressure. In addition, κ, the heat conductivity, c_p and c_v, the specific heats at constant pressure and volume, and their ratio, $\gamma \equiv c_p/c_v$ are assumed to be constant. The viscous dissipation function, Φ is defined as:

$$\Phi = \lambda(u_x + v_y)^2 + 2\mu(u_x^2 + v_y^2) + \mu(u_x + v_y)^2 \qquad (2.2)$$

and we shall use the Stokes relation, $\lambda + \frac{2}{3}\mu = 0$. The equation of state for an ideal gas,

$$T = \frac{1}{c_p - c_v} \frac{p}{\rho} \qquad (2.3)$$

is used. We now define the Prandtl number, $P_r \equiv \frac{c_p \mu}{\kappa}$, which will be used in what follows. Also the Reynolds number with respect to the length of the airfoil is defined as

$$R_l \equiv \frac{\rho_\infty U_\infty}{\mu} l \qquad (2.4)$$

where the subscript, ∞ implies that the "free-stream" value of the quantity is taken. In addition, the viscosity, μ is assumed to be constant.

Assume that the flow is external, and the length of the airfoil is l. Defining the dimensionless variables: $s = x/l$ and $z = y/l$, an approximate wake profile in the zero lift case can be obtained [3]:

$$\frac{u}{U_\infty} = 1 - m \frac{\sqrt{R_l}}{2\sqrt{\pi s}} e^{-R_l \frac{z^2}{4s}} \ . \qquad (2.5)$$

Integrating (2.5) we obtain an expression for m in terms of the drag coefficient, c_D:

$$m = \int_{-\infty}^{+\infty} (1 - \frac{u}{U_\infty}) \, dz = \frac{c_D}{2} \ . \qquad (2.6)$$

We substitute the above into (2.5) and make the following parabolic approximation:

$$\frac{u_0(z;s_0)}{U_\infty} \stackrel{def}{\equiv} \begin{cases} 1 - \frac{c_D\sqrt{R_l}}{4\sqrt{\pi s_0}}\left[1 - \frac{4R_l z^2}{9\pi s_0}\right] & \text{if} \quad z^2 < \frac{9\pi s_0}{4R_l} \equiv \frac{\delta^2}{l^2} \\ 1 & \text{if} \quad z^2 \geq \frac{9\pi s_0}{4R_l} \end{cases} \qquad (2.7)$$

where $x_0 = s_0 l$ is far enough from the airfoil so that the value of m using (2.5) will not change as $s > s_0$. Note that (2.7) satisfies (2.6), and defines an approximate wake thickness of:

$$\delta = \frac{3}{2}\sqrt{\frac{\pi s}{R_l}}.$$

Perturbing (2.1) in the region $y^2 < \delta^2$ around steady state conditions far downstream gives:

$$\begin{cases} \rho'_t + u_0(y)\rho'_x + \rho_\infty u'_x + \rho_\infty v'_y = 0 \\ \rho_\infty[u'_t + u_0(y)u'_x + (u_0)_y v'] + p'_x = \mu[u'_{xx} + u'_{yy}] + \frac{\mu}{3}[u'_x + v'_y]_x \\ \rho_\infty[v'_t + u_0(y)v'_x] + p'_y = \mu[v'_{xx} + v'_{yy}] + \frac{\mu}{3}[u'_x + v'_y]_y \\ p'_t + \gamma p_\infty u'_x + \gamma p_\infty v'_y + u_0(y)p'x = \\ \quad \frac{\gamma\mu}{P_r \rho_\infty}[(p'_{xx} + p'_{yy}) - \frac{p_\infty}{\rho_\infty}(\rho'_{xx} + \rho'_{yy})] + 2(\gamma - 1)(u_0)_y \mu[u'_y + v'_x] \end{cases} \qquad (2.8)$$

where: $u' = u - u_0$, $p' = p - p_0$, $\rho' = \rho - \rho_0$ and $v' = v$, and $p_0 = p_\infty$, $\rho_0 = \rho_\infty$, $v_0 = 0$, $u_0(y)$ is defined in (2.7). In addition, $\frac{\partial}{\partial x}(\cdot)_0 = \frac{\partial}{\partial t}(\cdot)_0 = 0$.

Let

$$K = 1 - \frac{c_d\sqrt{R_l}}{4\sqrt{\pi s}} \qquad (2.9)$$

then

$$u_0(y) = U_\infty[K + (1 - K)\frac{y^2}{\delta^2}]. \qquad (2.10)$$

Note that in the wake region, $0 < K < 1$ and outside of the wake region, $K = 1$. Also, we make the following dispersive wave ansatz:

$$\begin{bmatrix} \rho' \\ u' \\ v' \\ p' \end{bmatrix} = e^{i(\psi t + bx)} \begin{bmatrix} F_1(y) \\ F_2(y) \\ F_3(y) \\ F_4(y) \end{bmatrix}. \qquad (2.11)$$

Next, we non-dimensionalize in the following manner:

$$\begin{array}{lll} F_1 = \rho_\infty G_1 & F_2 = U_\infty G_2 & F_3 = U_\infty G_3 \\ F_4 = \rho_\infty U_\infty^2 G_4 & \psi = \frac{U_\infty \omega}{\delta} & b = \frac{\beta}{\delta} \\ \varepsilon = \frac{\nu}{U_\infty \delta} & y = \delta\eta & \frac{d}{dy} = \frac{1}{\delta}\frac{d}{d\eta} \end{array} \qquad (2.12)$$

5

where $\nu = \mu/\rho_\infty$ (kinematic viscosity). Substituting the ansatz and the non-dimensionalizations into (2.8) leads to the following set of dimensionless perturbations (similar to the Orr-Sommerfeld system) in the wake region $(-1 \le \eta \le 1)$.

$$i[\omega + \beta K(1 + (\frac{1-K}{K}\eta^2))]G_1 + i\beta G_2 + G_3' = 0$$
$$i[\omega + \beta K(1 + (\frac{1-K}{K}\eta^2))]G_2 + 2(1-K)\eta G_3 + i\beta G_4 = \varepsilon[G_2'' + i\frac{\beta}{3}G_3' - \frac{4}{3}\beta^2 G_2]$$
$$i[\omega + \beta K(1 + (\frac{1-K}{K}\eta^2))]G_3 + G_4' = \varepsilon[\frac{4}{3}G_3'' + i\frac{\beta}{3}G_2' - \beta^2 G_2]$$
$$i[\omega + \beta K(1 + (\frac{1-K}{K}\eta^2))]G_4 + \frac{i\beta G_2}{M_\infty^2} + \frac{G_3'}{M_\infty^2} =$$
$$\frac{\gamma\varepsilon}{P_r}[(G_4'' - \frac{G_1''}{\gamma M_\infty^2}) - \beta^2(G_4 - \frac{G_1}{\gamma M_\infty^2})] + 4(\gamma-1)(1-K)\varepsilon\eta[G_2' + i\beta G_3] \tag{2.13}$$

where $(\cdot)' = \frac{d\cdot}{d\eta}$.

We now perturb (2.13) around long wavelengths – *about small β*. To this end, we substitute:

$$G_i = G_i^{(0)} + \beta G_i^{(1)} + \beta^2 G_i^{(2)} + \cdots \quad (i = 1,2,3,4)$$
$$\omega = \omega_0 + \beta\omega_1 + \beta^2\omega_2 + \cdots \tag{2.14}$$

into (2.13), obtaining the following zeroth and first order problems:

The Zeroth Order Problem:

$$\begin{cases} g_1 - \varphi' = 0 \\ g_2'' + \Omega g_2 - 2(1-K)\eta\Omega\varphi = 0 \\ \varphi'' + \frac{3}{4}\Omega\varphi - \frac{3}{4}\psi' = 0 \\ g_1'' - 4(\gamma-1)(1-K)P_r M_\infty^2 \eta g_2' + P_r\Omega\varphi' - \gamma\varepsilon^2 M_\infty^2\Omega[\psi'' + \frac{\Omega P_r}{\gamma}\psi] = 0. \end{cases} \tag{2.15}$$

where $g_i \equiv G_i^{(0)}$, $i = 1,2,3,4$ together with the change of variables:

$$i\omega_0 = -\varepsilon\Omega \qquad g_3 = \varepsilon\Omega\varphi \qquad g_4 = \varepsilon^2\Omega\psi. \tag{2.16}$$

The First Order Problem:

$$\begin{cases} G_1 - \Phi' = \frac{i}{\Omega}g_2 + \frac{i}{\Omega}[\omega_1 + K(1 + \frac{1-K}{K}\eta^2)]g_1 \\ G_2'' + \Omega G_2 - 2\Omega(1-K)\eta\Phi = i[\omega_1 + K(1 + \frac{1-K}{K}\eta^2)]g_2 + i\Omega\varepsilon^2[\psi - \frac{1}{3}\varphi'] \\ \Phi'' + \frac{3}{4}\omega\Phi - \frac{3}{4}\Pi' = i\frac{3}{4}[\omega_1 + K(1 + \frac{1-K}{K}\eta^2)]\varphi - \frac{i}{4\Omega}g_2' \\ G_1'' - 4(\gamma-1)(1-K)P_r M_\infty^2 \eta G_2' + P_r\Omega\Phi' - \gamma\varepsilon M_\infty^2\Omega[\Pi'' + \frac{\Omega P_r}{\gamma}\Pi] = \\ \qquad\qquad -i\varepsilon^2 P_r M_\infty^2\Omega[\omega_1 + K(1 + \frac{1-K}{K}\eta^2)]\phi \\ \qquad\qquad -iP_r g_2 + 4\varepsilon^2 i(\gamma-1)(1-K)P_r M_\infty^2\eta\Omega\varphi \end{cases} \tag{2.17}$$

with the following change of variables:

$$G_1 = \varepsilon G_1^{(1)} \qquad G_2 = \varepsilon G_2^{(1)} \qquad \Phi = \frac{G_3^{(1)}}{\Omega} \qquad \Pi = \frac{G_4^{(1)}}{\varepsilon\Omega}. \tag{2.18}$$

6

In order to solve the zeroth and first order problems, appropriate boundary conditions need to be established. We shall derive these conditions by looking at the perturbations outside the wake region, $K = 1$, and then match at $\eta = \pm 1$. One can easily check that placing $K = 1$ in (2.13) gives a system with constant coefficients. We shall call the perturbations outside the wake region, Q, analogous to G in the wake region. Clearly this implies that Q_i takes the form $\hat{Q}_i e^{r\eta}$ with $\hat{Q}_i$ as constant. Now the *exact* boundary conditions for the zeroth and first order systems are $G_i(\pm 1) = Q_i(\pm 1), i = 1, 2, 3, 4$. In order to get a relationship on the G_i's we use the fact that they satisfy $\left[\frac{dQ_i}{d\eta}\right]_{\eta=\pm 1} = \left[\frac{dG_i}{d\eta}\right]_{\eta=\pm 1}$. Since also Q_i must satisfy $\left[\frac{dQ_i}{d\eta}\right]_{\eta=\pm 1} = [rQ_i]_{\eta=\pm 1}$ $i = 1, 2, 3, 4$, then clearly appropriate boundary conditions on $G_i(\pm 1)$ are:

$$\left[\frac{dG_i}{d\eta}\right]_{\eta=\pm 1} = [rG_i]_{\eta=\pm 1} \quad i = 1, 2, 3, 4. \tag{2.19}$$

In order to obtain r in the previous expression, we do the following:

Substituting $K = 1$ into (2.13) and using $Q_i = \hat{Q}_i e^{r\eta}$ and hence $Q_i' = rQ_i$, and $Q_i'' = r^2 Q_i$ we obtain:

$$\begin{cases} i(\omega + \beta)Q_1 + i\beta Q_2 + rQ_3 = 0 \\ (i(\omega + \beta) - \varepsilon r^2)Q_2 - i\beta \frac{\varepsilon}{3} rQ_3 + i\beta Q_4 = 0 \\ (i(\omega + \beta) - 43\varepsilon r^2)Q_3 - i\beta \frac{\varepsilon}{3} rQ_2 + rQ_4 = 0 \\ (i(\omega + \beta) - \frac{\gamma}{P_r}\varepsilon r^2)Q_4 + \frac{\varepsilon}{P_r M_\infty^2} r^2 Q_2 + \frac{i\beta}{M_\infty^2} Q_2 + \frac{r}{M_\infty^2} Q_3 = 0. \end{cases} \tag{2.20}$$

We expand Q_i and r around β as in (2.14) and define $Q_i^{(0)} = q_i$ and obtain the zeroth order problem in the free stream region:

$$\begin{cases} i\omega_0 q_1 + r_0 q_3 = 0 \\ (i\omega_0 - \varepsilon r_0^2)q_2 = 0 \\ (i\omega_0 - \frac{4}{3}\varepsilon r_0^2)q_3 + r_0 q_4 = 0 \\ \frac{\varepsilon}{P_r} r_0^2 q_1 + r_0 q_3 + (i\omega_0 - r_0^2 \frac{\gamma}{P_r}\varepsilon)M_\infty^2 q_4 = 0 \end{cases} \tag{2.21}$$

where it is evident that either $q_2 = 0$ or $r_0^2 = \frac{i\omega_0}{\varepsilon} = -\Omega$. We note that $e^{r\eta}$ cannot decay as $\eta \to \pm\infty$ if $r_0^2 = -\Omega$ hence $q_2 = 0$. For the rest of the system, the first, third and fourth equations in (2.21), we apply the existence criterion for nontrivial solutions of homogeneous systems, namely:

$$det \begin{pmatrix} i\omega_0 & r_0 & 0 \\ 0 & i\omega_0 - \frac{4}{3}\varepsilon r_0^2 & r_0 \\ \frac{\varepsilon}{P_r} r_0^2 & r_0 & M_\infty^2(i\omega_0 - \frac{\gamma}{P_r}\varepsilon r_0^2) \end{pmatrix} = 0 \tag{2.22}$$

We expand this around the first row retaining terms up to $O(\varepsilon^2 M_\infty^2)$. Assuming that $\frac{4}{3}\gamma\Omega\varepsilon^2 M_\infty^2 \ll 1$, then, we find that:

$$r_0^2 = \begin{cases} \Omega^2\varepsilon^2 M_\infty^2 \\ P_r\Omega[-1 + (\frac{4}{3} - \frac{\gamma-2}{2P_r})\Omega\varepsilon^2 M_\infty^2] \end{cases} \tag{2.23}$$

For subsonic flows with $\gamma = 1.4$ and $P_r = 0.72$ and small ε (physically reasonable) the latter result is negative. Hence the perturbations will not decay in η. Therefore, we choose:

$$r_0 = \mp\Omega M_\infty\varepsilon \tag{2.24}$$

where the $-$ sign is taken for positive η and the $+$ sign is taken for negative η, so that the perturbations in free-stream will die out in η.

The first order problem in the free stream region takes the form:

$$\begin{cases} i\omega_0 Q_1^{(1)} + r_0 Q_3^{(1)} = -i(\omega_1 + 1)q_1 - r_1 q_3 \\ (i\omega_0 - \varepsilon r_0^2)Q_2^{(1)} = i\frac{\varepsilon}{3}r_0 q_3 - iq_4 \\ (i\omega_0 - \frac{4}{3}\varepsilon r_0^2)Q_3^{(1)} + r_0 Q_4^{(1)} = (-i(\omega_1 + 1) + \frac{8}{3}\varepsilon r_0 r_1)q_3 - r_1 q_4 \\ \frac{\varepsilon}{P_r}r_0^2 Q_1^{(1)} + r_0 Q_3^{(1)} + (i\omega_0 - \frac{\gamma}{P_r}\varepsilon r_0^2)M_\infty^2 Q_4^{(1)} = \\ \qquad (-i(\omega_1 + 1) + \frac{2\gamma}{P_r}\varepsilon r_0 r_1)M_\infty^2 q_4 - \frac{2\varepsilon r_0 r_1}{P_r}q_1 - r_1 q_3 \,. \end{cases} \tag{2.25}$$

The r_0 chosen above makes the coefficient determinant of the left-hand-side singular. Hence, solvability here requires that the same coefficient determinant with one of its columns replaced by the right-hand-side be singular as well. This criterion leads to:

$$r_1 = \pm i(\omega_1 + 1)M_\infty + O(\varepsilon^2 M_\infty^2). \tag{2.26}$$

In order to fix the boundary conditions for (2.15) and (2.17), we recall the requirement that:

$$\left[\frac{dG_i}{d\eta}\right]_{\eta=\pm 1} = [rG_i]_{\eta=\pm 1} \qquad i = 1, 2, 3, 4$$

whose β expansion is

$$\frac{d}{d\eta}\left[G_i^{(0)} + \beta G_i^{(1)} + \cdots\right]_{\eta=\pm 1} = \left[(r_0 + \beta r_1 + \cdots)(G_i^{(0)} + \beta G_i^{(1)} + \cdots)\right]_{\eta=\pm 1}$$

gives

$$\begin{cases} G_i^{(0)'}(\pm 1) = r_0 G_i^{(0)} \\ G_i^{(1)'}(\pm 1) = r_0 G_i^{(1)}(\pm 1) + r_1 G_i^{(0)} \,. \end{cases} \tag{2.27}$$

This, together with $q_2 = 0 \leftrightarrow g_2(\pm 1) = 0$ provides us with appropriate boundary conditions for the zeroth and first order perturbation problems. The reader will note

8

that the systems (2.15) and (2.17) are of order six, so only six conditions will be prescribed for them. For physical reasons, we do not place conditions on the pressure perturbations, i.e on ψ and on Π.

In summary, the boundary conditions on (2.15) are:

$$g_1'(\pm 1) = r_0 g_1(\pm 1)$$
$$g_2(\pm 1) = 0$$
$$\varphi'(\pm 1) = r_0 \varphi(\pm 1)$$

$$(2.28)$$

and on (2.17) are:

$$G_1'(\pm 1) = r_0 G_1(\pm 1) + \varepsilon r_1 g_1(\pm 1)$$
$$G_2'(\pm 1) = r_0 G_2(\pm 1)$$
$$\Phi'(\pm 1) = r_0 \Phi(\pm 1) + \varepsilon r_1 \varphi(\pm 1)$$

$$(2.29)$$

Since the perturbations decay like $e^{-\varepsilon \Omega t}$, we solve the zeroth order problem for its minimal positive Ω and then use this Ω in the first order problem to find ω_1 using a Fredholm like process. Since $\frac{d\omega}{d\beta}|_{\beta=0} = \omega_1$, then ω_1 has the physical meaning of being the group velocity of the longest waves.

3 The Incompressible Case

In this section we shall find appropriate Ω and ω_1 in the special case of incompressible viscous flows, i.e. $M_\infty = 0$.

3.1 The Time Consistent Case

The zeroth order problem in this case is:

$$\begin{cases} g_1 - \varphi' = 0 \\ g_2'' + \Omega g_2 - 2(1-K)\eta\omega\varphi = 0 \\ \varphi'' + \frac{3}{4}\Omega\varphi - \frac{3}{4}\psi' = 0 \\ g_1'' + \Omega P_r \varphi' = 0 \end{cases} \quad \begin{array}{l} g_1'(\pm 1) = 0 \\ g_2(\pm 1) = 0 \\ \varphi'(\pm 1) = 0 \end{array} \qquad (3.1)$$

whose normalized solution, in the sense that $\| g_2 \|_{L^2_{(-1,1)}} = 1$ is as follows:

$$g_1 = \varphi = \psi = 0 \qquad g_2(\eta) = cos(\frac{\pi}{2}\eta) \qquad (3.2)$$

hence:

$$0 < \Omega_{min} = \frac{\pi^2}{4} . \qquad (3.3)$$

9

The first order problem is interesting in that looking at (2.29) one would think that the appropriate boundary conditions on $G_2(\eta)$ are $G'_2(\pm 1) = 0$ making the usage of the *Fredholm alternative* incorrect. It can be easily shown that in fact:

$$
\begin{cases}
G_1 - \Phi' = \frac{i}{\Omega} g_2 \\
G''_2 + \Omega G_2 - 2\Omega(1 - K)\eta\phi = i[\omega_1 + K(1 + \frac{1-K}{K}\eta^2)]g_2 \\
\Phi'' + \frac{3}{4}\omega\Phi - \frac{3}{4}\Pi' = -\frac{i}{4\Omega} g'_2 \\
G'''_1 + P_r\Omega\Phi' = -iP_r g_2
\end{cases}
\qquad
\begin{aligned}
G'_1(\pm 1) &= 0 \\
G_2(\pm 1) &= 0 \\
\Phi'(\pm 1) &= 0
\end{aligned}
\qquad (3.4)
$$

so that left-hand-null-vector of the first order problem is indeed $cos(\frac{\pi}{2}\eta)$. Taking the scaler product of $cos(\frac{\pi}{2}\eta)$ and the second equation in (3.4) gives

$$
\omega_1 = -K - (1 - K)(\frac{1}{3} - \frac{6}{\pi^2}). \qquad (3.5)
$$

It should be made clear at this point that had the condition $g'_2(\pm 1) = 0$ been used instead of $g_2(\pm 1) = 0$, in the zeroth order problem, we would have found that $g_2(\eta) = sin(\frac{\pi}{2}\eta)$. In this case we would not have been able to solve the first order system for ω_1. So it is very important to identify the proper boundary conditions in order to assure finding Ω and ω_1.

The longwave expansion asymptotics done thus far are based on the assumption that the system of partial differential equations are solved in a time consistent manner using a global time marching scheme. In addition, had we started with the viscous incompressible boundary layer equations

$$
\begin{cases}
u_x + v_y = 0 \\
u_t + (u^2)_x + (uv)_y = \nu u_{yy}
\end{cases}
\qquad (3.6)
$$

and done the same type of longwave asymptotics as in §2 (note that the far-field profile, (2.7) is appropriate for this case as well) we would have obtained the same Ω and ω_1 as above. This means that essentially we have found the eigenvalues for the viscous incompressible boundary layer equations for time consistent numerical schemes. In the next subsection, we shall find these eigenvalues when local time stepping is to be used.

3.2   The Local Time Stepping Case

Many researchers use local time stepping in numerical marching schemes towards steady state. While local time stepping is not time consistent, it has been found to accelerate convergence to steady state.

We return to the viscous incompressible flat-plate boundary layer equations, (3.6).

10

We are interested in integrating this system numerically. In order to ensure numerical stability, the Courant Fredrichs Levy (CFL) condition on the time step for each grid node requires (see [7]) that Δt be bounded by some function of Δx_{ij} and Δy_{ij}. The function depends upon the numerical scheme used. In our numerical experiments Runge Kutta schemes were used. We were conservative in our approach and required that

$$\Delta t \leq \min_{ij} \Delta \theta_{ij} \tag{3.7}$$

where

$$\Delta \theta_{ij} \leq \min \left\{ \frac{\Delta x_{ij}}{u_{ij} + 1}, \beta \frac{(\Delta y_{ij})^2}{2\nu} \right\} \tag{3.8}$$

where $0 < \beta \leq 1$. The addition of the factor β helped stabilize the numerical iterative process. For the runs with global time stepping on a grid with constant Δx and Δy, $\beta = 1$ was enough for stability. however for the runs on a grid with nonconstant Δy, we chose $\beta = \frac{1}{2}$ to achieve stability (see §5).

Local time stepping means that at the node (x_{ij}, y_{ij}) a time step of $\Delta \theta_{ij}$ is chosen. Using local time stepping one discretizes the temporal derivatives in the following manner:

$$\left(\frac{\partial u}{\partial t} \right)_{ij} \approx \frac{u_{ij}^{n+1} - u_{ij}^n}{\Delta \theta_{ij}} . \tag{3.9}$$

Suppose we discretize (3.6) on a non-uniform rectangular grid and temporally discretize as in (3.9). Provided that the spatial derivatives are discretized consistently, $\frac{\partial (\Delta x)_{ij}}{\partial t} = \frac{\partial (\Delta y)_{ij}}{\partial t} = 0$, signifying that the grid is not changing in time. Therefore, these spatial discretizations are in fact valid approximations for the spatial derivatives. However, the temporal derivative is quite different. Since

$$\frac{u_{ij}^{n+1} - u_{ij}^n}{\Delta \theta_{ij}} = \left(\frac{\Delta t}{\Delta \theta_{ij}} \right) \frac{u_{ij}^{n+1} - u_{ij}^n}{\Delta t}$$

we clearly see that what we are approximating is in fact

$$\lim_{\Delta t \to 0} \left(\frac{\Delta t}{\Delta \theta_{ij}} \right) \frac{\partial u}{\partial t}. \tag{3.10}$$

Suppose that the grid was constructed so that in the boundary layer,

$$\Delta \theta_{ij} = \beta \frac{(\Delta y_{ij})^2}{2\nu} \tag{3.11}$$

and that the grid is geometrically expanding in the y direction so that

$$\Delta y_{ij} = k^{j-1} \Delta y_{i1}; \qquad k \geq 1$$

11

then

$$\left(\frac{\Delta t}{\Delta \theta_{ij}}\right) = \left(\frac{\Delta y_{i1}}{\Delta y_{ij}}\right)^2$$

and therefore

$$\lim_{\Delta t \to 0}\left(\frac{\Delta t}{\Delta \theta_{ij}}\right) = \frac{k^2}{\left[1 + \frac{y}{\Delta y_{i1}}(k-1)\right]^2} \stackrel{def}{=} F(y;k). \tag{3.12}$$

Note that $0 < F(y;k) < 1$ when $k > 1$ and that $F(y;1) = 1$.

Therefore, while we are solving (3.6) on this special grid using local time stepping, we are in actuality solving the modified system:

$$\begin{cases} u_x + v_y = 0 \\ F(y;k)u_t + (u^2)_x + (vu)_y = \nu u_{yy} \end{cases} \tag{3.13}$$

We shall now carry out a long-wave asymptotic analysis for the above system of equations. We note that the far-field wake profile, (2.5) is still appropriate in this case. Hence, using the parabolic far-field approximation for the wake profile (2.7) we again define the primed variables

$$u' = u - u_0 \qquad v' = v \ .$$

Perturbing (3.13) around steady state variables retaining linear terms in primed variables and substituting the dispersive wave ansatz:

$$\begin{bmatrix} u' \\ v' \end{bmatrix} = e^{i(\psi t + bx)} \begin{bmatrix} F_1(y) \\ F_2(y) \end{bmatrix} \tag{3.14}$$

and nondimensionalizing ψ, b, ε, and y as in (2.12) we obtain the following system of ordinary differential equations in η:

$$\begin{aligned} & iG_1(\eta)\beta + G_2'(\eta) = 0 \\ & i[\hat{F}(\eta;k)\omega + \beta K(1 + \tfrac{1-K}{K}\eta^2)]G_1(\eta) \\ & \qquad\qquad + 2G_2(\eta)(1-K)\eta = \varepsilon G_1''(\eta) \end{aligned} \tag{3.15}$$

where $F_1 = U_\infty G_1$ and $F_2 = U_\infty G_2$ and

$$\hat{F}(\eta;k) = \begin{cases} \dfrac{k^2}{\left[1 + \frac{\delta\eta}{\Delta y_{i1}}(k-1)\right]^2} & |\eta| < 1 \\[4mm] 1 & |\eta| \geq 1 \end{cases} \tag{3.16}$$

Perturbing G_i and ω about β:

$$\begin{aligned} & G_i = G_i^{(0)} + \beta G_i^{(1)} + \beta^2 G_i^{(2)} + \cdots \quad (i = 1,2,3,4) \\ & \omega = \omega_0 + \beta\omega_1 + \beta^2\omega_2 + \cdots \end{aligned} \tag{3.17}$$

12

and substituting these perturbations into (3.15) we get the following zeroth and first order problems in β:

The Zeroth Order Problem:

$$\begin{cases} \varphi'(\eta) = 0 \\ g_1'' + \Omega \hat{F}(\eta; k) g_1 - 2(1 - K) \eta \Omega \varphi = 0 \end{cases} \tag{3.18}$$

where $G_i^{(0)} = g_i$, $g_2 \equiv \varepsilon \Omega \varphi$ and $i w_0 = -\Omega \varepsilon$.

The First Order Problem:

$$\begin{cases} \Phi' = -\frac{i}{\Omega} g_1 \\ \hat{G}_1'' + \Omega \hat{F}(\eta; k) G_1 - 2\Omega \Phi (1 - K) \eta = \\ \qquad i g_1 \left[\hat{F}(\eta; k) \omega_1 + K \left(1 + \left(\frac{1-K}{K} \right) \eta^2 \right) \right] \end{cases} \tag{3.19}$$

where $\hat{G}_1 = \varepsilon G_1^{(1)}$ and $\Psi = \frac{G^{(1)}}{\Omega}$.

Again, we need to match solutions at $|\eta| = 1$ (at the boundary of the wake region) — when $K = 1$. Formally setting $k = 1$ because out of the wake region the grid stretching should have no effect either on Ω or on ω_1 we obtain the linear perturbation system in the free stream region:

$$\begin{cases} i G_1(\eta) \beta + G_2'(\eta) = 0 \\ i \left[\omega + \beta \right] G_1(\eta) = \varepsilon G_1''(\eta) \end{cases} \tag{3.20}$$

whose constant coefficients imply a solution of the form:

$$\begin{bmatrix} G_1 \\ G_2 \end{bmatrix} = e^{r\eta} \begin{bmatrix} \hat{G}_1(\eta) \\ \hat{G}_2(\eta) \end{bmatrix} \tag{3.21}$$

Expanding as before, around β

$$\hat{G}_i = \hat{g}_i + \beta \hat{G}_i^1 + \cdots$$
$$r = r_0 + \beta r_1 + \cdots$$
$$\omega = \omega_0 + \beta \omega_1 + \cdots$$

we obtain the following zeroth and first order problems in the free stream region:

$$\underline{0^{th} \ order \ (\beta^0):} \qquad \begin{matrix} r_0 \hat{g}_2 = 0 \\ (i w_0 - \varepsilon r_0^2) \hat{g}_1 = 0 \end{matrix} \tag{3.22}$$

13

from which immediately $\hat{g}_2 = 0$. Since $i\omega_0 = -\varepsilon\Omega$ then $\hat{g}_1 = 0$ as well, otherwise the perturbations will not decay in η.

$$\underline{1^{st} \ order \ (\beta^1)}: \qquad i\hat{g}_1 + r_0 \hat{G}_2^1 + r_1 \hat{g}_2 = 0$$
$$\hat{G}_1^1 (i\omega_0 - \varepsilon r_0^2) = 0 \qquad\qquad (3.23)$$

As in the zeroth order problem above, both $\hat{G}_1^1 = 0$ and $\hat{G}_2^1 = 0$.

This implies that the boundary conditions for the zeroth order problem are

$$g_1(\pm 1) = 0$$
$$\varphi(\pm 1) = 0 \qquad\qquad (3.24)$$

and that the boundary conditions for the first order problem are

$$G_1(\pm 1) = 0$$
$$\Phi(\pm 1) = 0 \ . \qquad\qquad (3.25)$$

Notice that the zeroth order problem reduces to:

$$g_1'' + \Omega \hat{F}(\eta; k) g_1 = 0$$
$$g_1(\pm 1) = 0 \qquad\qquad (3.26)$$

Since $0 < \hat{F}(\eta; k) < 1$ when $k > 1$ then the Sturm Comparison and Oscillation theorems (see [4]) indicate that the minimal positive eigenvalue Ω in (3.26) will be greater than the minimal positive eigenvalue in the non-stretched incompressible case. This fact is crucial and to a certain extent indicates why local time stepping is so effective. Since it is believed that indeed the long wave perturbations are the slowest to converge to steady state, then we have just shown that the decay of these disturbances is faster in local time stepping regimes than in global time stepping regimes.

In (§5) we present numerical evidence indicating that the nonreflecting boundary condition is quite effective in local time stepping regimes indicating that the absorbed long waves do in fact decay as we predict. This is an interesting illustration of one of the reasons why local time stepping is effective.

4   Derivation of the Far-Field Non-Reflecting Boundary Condition

Once the two eigenvalues, Ω and ω_1 are found, an appropriate far-field boundary condition can be developed to accommodate the physical situation at the far-field.

4.1 Derivation for Single-Grid Numerical Methods

From the ansatz (2.11), we have:

$$p' = e^{i(\psi t + bx)} \rho_\infty U_\infty^2 G_4$$

Substituting the dimensionless temporal and spatial variables: into the profile, we obtain (up to order β):

$$p = e^{is_0 \frac{l}{\delta}(\omega_0 \theta + \omega_1 \beta \theta + \beta \xi)} \rho_\infty U_\infty^2 G_4(\eta) + p_\infty.$$

Taking a derivative with respect to θ and using the identity $is_0 \frac{l}{\delta}\omega_0 = -\frac{4}{9\pi}\Omega$, we arrive at the far-field boundary condition:

$$\frac{\partial p}{\partial \theta} = -\frac{4}{9\pi}\Omega(p - p_\infty) + \omega_1 \frac{\partial p}{\partial \xi}. \tag{4.1}$$

In the incompressible case where $\Omega = \frac{\pi^2}{4}$, the condition takes the form:

$$\frac{\partial p}{\partial \theta} = -\frac{\pi}{9}(p - p_\infty) + \omega_1 \frac{\partial p}{\partial \xi}. \tag{4.2}$$

4.2 Derivation for Numerical Methods Utilizing Multigrid Acceleration

The non-reflecting boundary condition just developed was based upon an analysis around long waves. Should multigrid acceleration be used in conjunction with the numerical scheme then short waves must be taken into account as well. Substituting P for $p - p_\infty$, the boundary condition (4.1) may be rewritten as

$$\frac{\partial P}{\partial t} = -\frac{4}{9\pi}\Omega P + \omega_1 \frac{\partial P}{\partial x}. \tag{4.3}$$

Taking the Fourier transform in x of the above equation we obtain

$$\hat{P}_t = -\frac{4}{9\pi}\Omega \hat{P} + ik\omega_1 \hat{P}. \tag{4.4}$$

which has the general solution:

$$\hat{P} = \mathcal{C}e^{(-\frac{4}{9\pi}\Omega + ik\omega_1)t}.$$

For short waves, or high Fourier modes, k, the highly oscillatory behaviour of the symbol $\hat{P}$ with t, will cause short wave disturbances in the numerical solution. This

is especially critical when using multigrid techniques whose goal on each grid is to damp short waves. Our original nonreflecting boundary condition, while effective in damping long wave disturbances caused by reflections, may create new short wave disturbances and destroy the effects of the multigrid acceleration.

By replacing ik in (4.4) with

$$\frac{ik}{1 + ik}$$

we obtain a new Fourier symbol free of oscillatory behaviour even as k gets large:

$$\hat{P} = C e^{(-\frac{4}{9\pi}\Omega + \frac{ik}{1+ik}\omega_1)t}. \tag{4.5}$$

The symbol (4.5) comes from the equation:

$$\hat{P}_t = -\frac{4}{9\pi}\Omega\hat{P} + \frac{ik}{1 + ik}\omega_1\hat{P} . $$

Transforming back to the original variables we obtain the boundary condition to be used with multigrid acceleration:

$$\frac{\partial p}{\partial t} = -\frac{4\Omega}{9\pi}(p - p_\infty) + \omega_1\frac{\partial p}{\partial x} - \frac{\partial}{\partial x}\left[\frac{\partial p}{\partial t} + \frac{4}{9\pi}\Omega(p - p_\infty)\right] \tag{4.6}$$

or

$$\left(1 + \frac{\partial}{\partial x}\right)\frac{\partial p}{\partial t} = -\frac{4\Omega}{9\pi}(p - p_\infty) + \left[\omega_1 - \frac{4\Omega}{9\pi}\right]\frac{\partial p}{\partial x}. \tag{4.7}$$

5 Numerical Results

In this section we present various numerical results obtained using the far-field boundary condition just derived. We break this section into three subsections. The first describes the numerical technique for calculating Ω and ω_1 in compressible cases. The second section deals with the numerical solution of the incompressible boundary layer equations both with global and local time stepping. The third presents the results obtained in compressible viscous flows around the NACA0012 airfoil using global time stepping regimes with and without multigrid acceleration.

5.1 The numerical calculation of Ω and ω_1 in the global time stepping case

The discretized form of the zeroth order problem (2.15, 2.28) is a generalized eigenvalue problem:
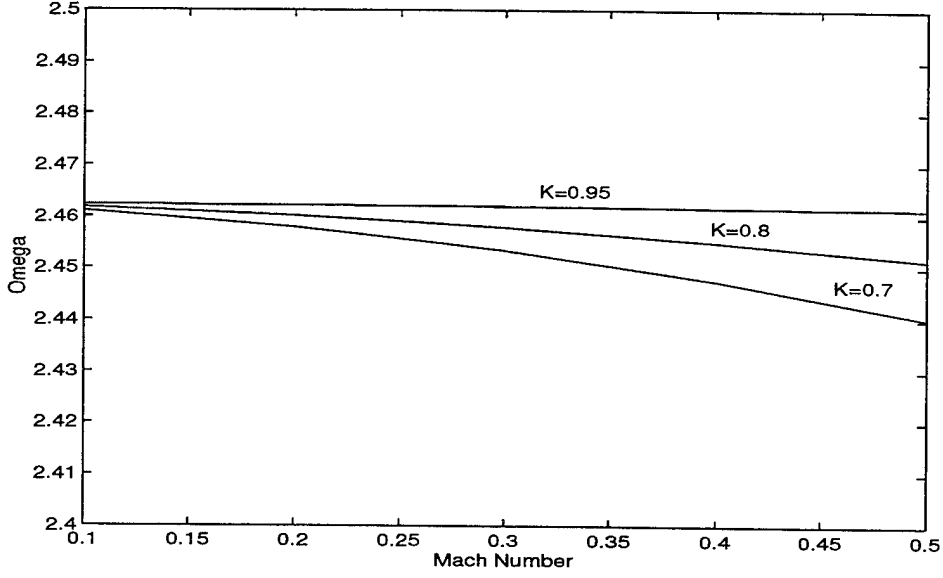
$$A\vec{x} = h^2\Omega B(\Omega)\vec{x} \tag{5.1}$$

16

Figure 3: Ω versus M_∞ for $K = 0.7, 0.8, 0.95$

where h is the cell size, $\Delta\eta$, and $\vec{x}$ is $(g^1, g^2, \varphi, \psi)$. The problem is non-linear since $B = B(\Omega)$ is a function of Ω, so the following iterative scheme was used:

$$\left\{ \begin{array}{l} \Omega^0 = \frac{\pi^2}{4} \\ A\vec{x} = h^2 \Omega^{n+1} B(\Omega^n)\vec{x} \end{array} \right. \tag{5.2}$$

where at each iteration, the smallest positive Ω was determined. Generally convergence was obtained after three iterations and the main result is (Figure 3):

For all physically relevant values of ε, M_∞ and K (see eq. 2.9);
$\Omega = \frac{\pi^2}{4}$.

The discrete first order problem (2.17, 2.29) can be written in the form:

$$C(\Omega)\vec{X} \equiv (\tilde{A} - h^2 \Omega \tilde{B}(\Omega))\vec{X} = \vec{\mathcal{R}}_1 + \omega_1 \vec{\mathcal{R}}_2 \tag{5.3}$$

where $\vec{X} = (G_1, G_2, \Phi, \Psi)$ and where $A \leftrightarrow \tilde{A}$ and $B \leftrightarrow \tilde{B}$ *except* that the boundary conditions on g_2 are not parallel to those on G_2. The technique used to obtain ω_1 was to find the left hand null vector of $C(\Omega)$, $\vec{v}$, and then

$$\omega_1 = -\frac{(\vec{v}, \vec{\mathcal{R}}_1)}{(\vec{v}, \vec{\mathcal{R}}_2)}. \tag{5.4}$$

Unlike Ω, ω_1 was not found to be constant for all physically relevant parameters. Figure 4 graphically shows the values of ω_1 as a function of $1 - K$ for $M_\infty = 0, 0.1, 0.2, 0.3$ (for neatness $M_\infty = 0.4, 0.5$ were not shown). The main result is:
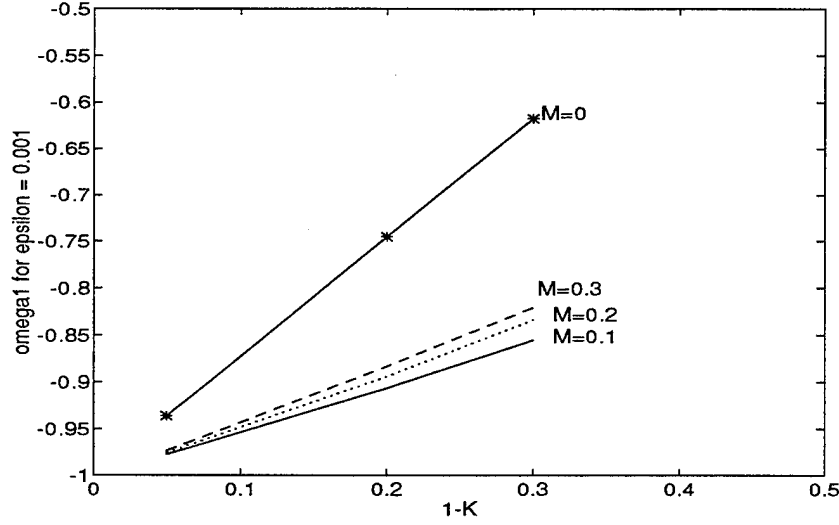
17

Figure 4: ω_1 versus $1 - K$ for $\varepsilon = .001$

$\omega_1 \xrightarrow{K \to 1} -1$ *for* $0 < M \leq 0.5$ *and for all physical* ε.

The limit $M_\infty \to 0$ *is singular.*

In Table 1 values of Ω and ω_1 for a variety of parameters, ε, M_∞ and K for time consistent numerical integration schemes are listed. These values were obtained through a program written in MATLAB.

5.2   Incompressible Viscous Flow

5.2.1   Case 1- Global Time Stepping Regimes

The viscous incompressible boundary layer equations (for a flat plate) (3.6) have been solved in the geometry of Figure 2. The Reynolds number (with respect to the plate length), R_l, taken was 100000, and a rectangular grid (476x61) with cell aspect ratio, $\frac{\Delta x}{\Delta y}$, of 25 was used. The plate had 76 nodes in the x direction, and there were 400 x nodes in the wake region. At inflow, one quarter the way down the flat plate, a Blasius profile was placed. The outflow boundary was placed four plate-lengths from the trailing edge. The momentum equation was integrated in time using a Runga-Kutta scheme as suggested by [6], where the first order spatial derivatives were discretized using a compact fourth-order scheme developed by Abarbanel et. al. [2]. The second derivatives were discretized using standard second-order central differencing.

18

K	ε	M_∞	Ω	ω_1
0.950000	0.000100	0.100000	2.462296	-0.979065
0.950000	0.001000	0.100000	2.462296	-0.977492
0.950000	0.000100	0.200000	2.462190	-0.979052
0.950000	0.001000	0.200000	2.462185	-0.975585
0.950000	0.000100	0.300000	2.462014	-0.978915
0.950000	0.001000	0.300000	2.461997	-0.973317
0.950000	0.000100	0.400000	2.461773	-0.978703
0.950000	0.001000	0.400000	2.461732	-0.982999
0.950000	0.000100	0.500000	2.461471	-0.977015
0.950000	0.001000	0.500000	2.461392	-0.967744
0.800000	0.000100	0.100000	2.461776	-0.911913
0.800000	0.001000	0.100000	2.461767	-0.906617
0.800000	0.000100	0.200000	2.460254	-0.904457
0.800000	0.001000	0.200000	2.460203	-0.894001
0.800000	0.000100	0.300000	2.458007	-0.897642
0.800000	0.001000	0.300000	2.457900	-0.883191
0.800000	0.000100	0.400000	2.455157	-0.892715
0.800000	0.001000	0.400000	2.455005	-0.875650
0.800000	0.000100	0.500000	2.451718	-0.892979
0.800000	0.001000	0.500000	2.451536	-0.870731
0.700000	0.000100	0.100000	2.461120	-0.862841
0.700000	0.001000	0.100000	2.461103	-0.855154
0.700000	0.000100	0.200000	2.458011	-0.847079
0.700000	0.001000	0.200000	2.457942	-0.833530
0.700000	0.000100	0.300000	2.453518	-0.840599
0.700000	0.001000	0.300000	2.453408	-0.820463
0.700000	0.000100	0.400000	2.447673	-0.835958
0.700000	0.001000	0.400000	2.447541	-0.814361
0.700000	0.000100	0.500000	2.440383	-0.834136
0.700000	0.001000	0.500000	2.440236	-0.812478

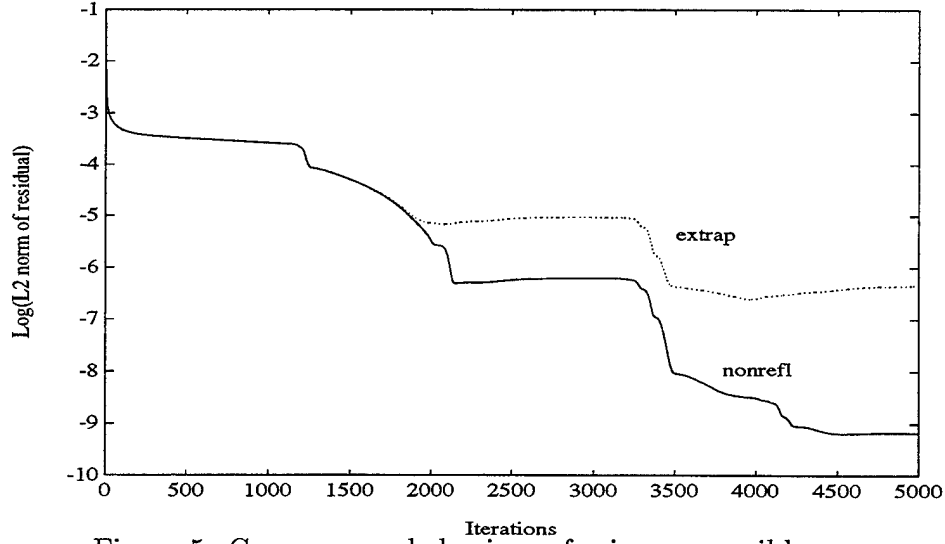Table 1: Ω and ω_1 for various K, ε, and M_∞

Figure 5: Convergence behaviours for incompressible case.

Two cases were run. The first with extrapolation of u at outflow, and the second using our far-field boundary condition (incompressible, (4.2)) at outflow with ω_1 updated every iteration as in (3.5). In each case 5000 time steps were taken. Figure 5 shows the convergence behaviour. It is evident that the non-reflecting condition reduced markedly the residuals in the flow field, implying that the the non-refleflecting boundary condition produced a more stable numerical solution than did extrapolation.

In order to test the effect of the nonreflecting boundary condition as the outflow boundary is moved closer to the trailing edge, additional runs were performed with the outflow boundary at $s = 2$ and at $s = 3$. Figure 7 shows that as s decreases, the effects of the nonreflecting boundary condition are more dramatic. In addition, Call S2, S3, and S4 the solutions of the flatplate problem on grids $G2 \subset G3 \subset G4$ respectively. Use N as an extention for a case with the nonreflecting boundary conditions at outflow, and use E as an extention for a case with extrapolation conditions at outflow. We looked to see to what degree

$$SN2 \subset SN3 \subset SN4,$$

and

$$SE2 \subset SE3 \subset SE4.$$

It turns out that $SN2 \subset SN3 \subset SN4$ up to four significant digits whereas $SE2 \subset SE3 \subset SE4$ only up to two significant digits. Hence, we are certain that our boundary condition maintains accuracy better than the extrapolation condition does. All of
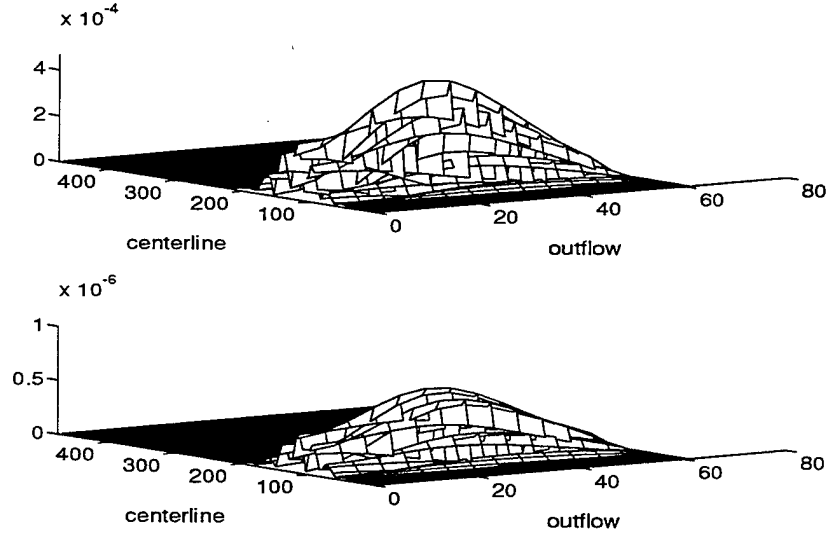
20

Figure 6: Residuals after 5000 time steps - Extrapolation (top) Non-reflecting (bottom)

this indicates that one could use a smaller computational domain while using the non-reflecting boundary condition and maintain "large computational domain" accuracy, thereby dramatically reducing the amount of computational work needed.

5.2.2 Case 2- Local Time Stepping Regimes

We shall now describe the results obtained using the nonreflecting boundary condition in conjunction with a local time stepping regime. Let us state the conditions of the case studied.

(1) The Grid: As in subsubsection 5.2.1, the global time stepping case, the equations are discretized on a 476×61 rectangular grid. The inflow boundary is located one quarter away down the flat plate and the outflow boundary is placed 4 chord lengths down stream from the trailing edge. While Δx is constant, Δy grows geometrically so that $\Delta y_{i,j} = k^{j-1}\Delta y_{i,1}$, where $\Delta y_{i,j} \equiv y_{i,j} - y_{i,j-1}$. The expansion factor, k, was chosen so that in 60 intervals, y reaches one chord length. It should be noted that the aspect ratio of cells above the plate and the centerline are set identical to those in the global time step case so that in the local time stepping case Δt is determined by the parabolic part of the system in most of the wake region, recall (3.11).

(2) Physical conditions: In this case, R_l is again taken to be 100000. Also, the boundary condition at inflow is the Blasius profile one-quarter way down the plate. The outflow boundary is located 4 chord-lengths away from the trailing edge. Equa-
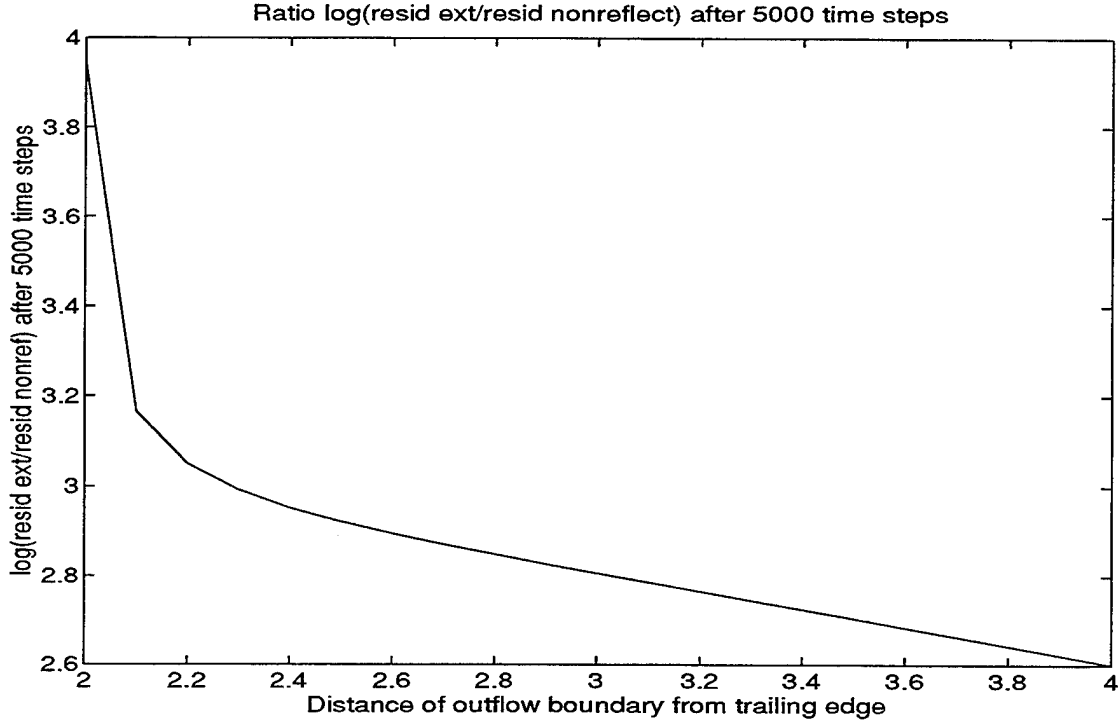
21

Figure 7: The ratio $log_{10}\left(\dfrac{\text{final residual with extrapolation bc}}{\text{final residual with nrbc}}\right)$ after 5000 iterations as a function of the distance of the outflow boundary from the trailing edge of a flat plate.

tions (3.18) and (3.19) with their boundary conditions, (3.24) and (3.25) are numerically solved in this case for Ω and ω_1 using a program written in Mathematica. The algorithm is similar to the the one presented in subsection 5.1. In this case, Ω is not a constant and depends upon the expansion factor, k. For these physical conditions we obtain

$$\Omega = 5.95497$$

which is significantly larger than $\frac{\pi^2}{4}$, obtained in the global time stepping case. This implies that the long wave disturbances decay faster when local time steps are used than with global time steps. Regarding ω_1, recall that in the global time stepping scheme case the relationship between between ω_1 and K was linear. Therefore, the relationship between ω_1 and c_d was linear as well. It has been numerically determined for the present local time stepping case, that the relationship between ω_1 and c_d is linear as well, more specifically:
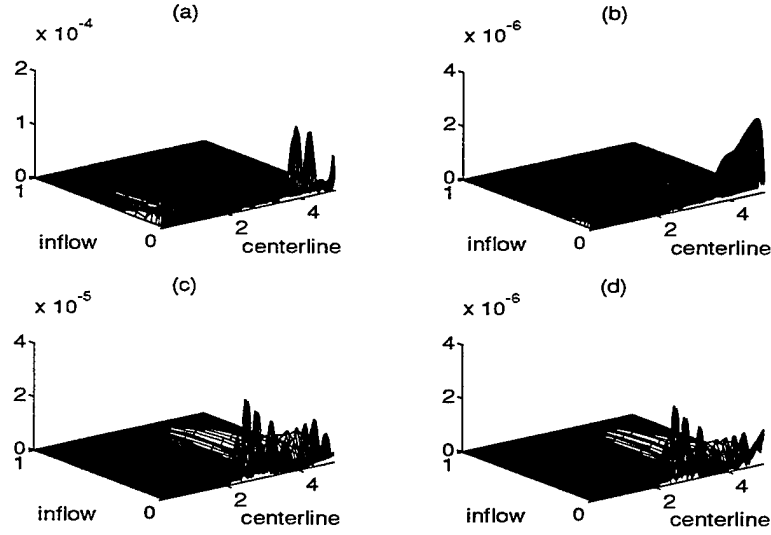
22

Figure 8: Residual plots after 5000 iterations (a) extrapolation, gts (b) non-reflecting condition, gts (c) extrapolation, lts (d) non-reflecting, lts

$$\omega_1 = 56.32c_d - 2.01413 \ . \tag{5.5}$$

The non-reflecting boundary condition with these coefficients was used as an outflow boundary condition, as was extrapolation. The results were compared and we state them now.

In figure (8) the pointwise residuals after 5000 iterations for the four test cases (extrapolation outflow conditions–global time stepping, non-reflecting outflow conditions–global time stepping, extrapolation outflow conditions–local time stepping, and non-reflecting outflow conditions–local time stepping). are plotted. In figure 9 the L^2 norm of the residuals (for each case) is plotted as a function of time steps. Figure 9 (a) graphs the logarithm of the L^2 norm of the residual as a function of time steps (iterations) for global time stepping runs. Figure 9 (b) graphs the logarithm of the L^2 norm of the residuals as a function of time steps for local time steping runs. The bottom dotted line is a special case that will be discussed later on in this section. It is clear from the results that

- Local time stepping regimes converge faster than their global time stepping counterparts.

- The case with non-reflecting outflow conditions with global time stepping reaches steady state faster than the case with extrapolation outflow conditions and local
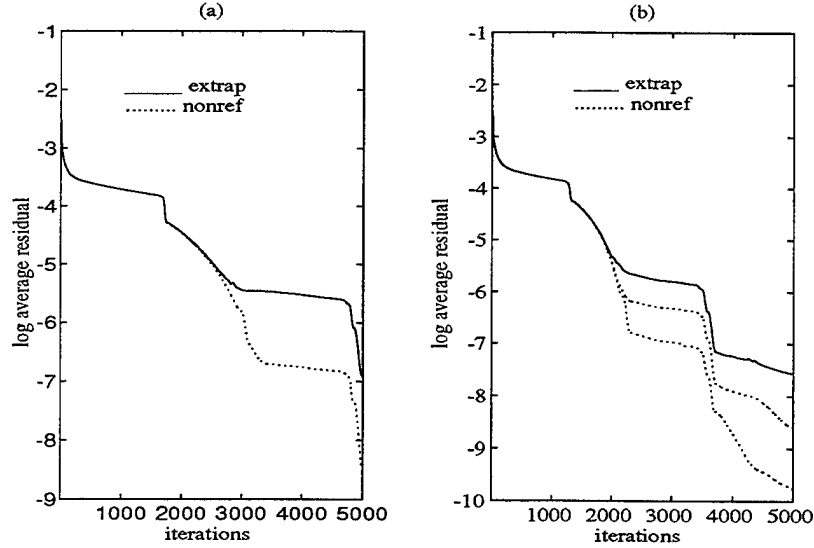
23

Figure 9: Residuals (a) global time stepping (b) local time stepping

time stepping.

Note that adding the non-reflecting boundary condition to the local time stepping scheme speeds up the convergence. This implies that the non-reflecting boundary condition accelerates convergence to steady state above and beyond local time stepping.

For experimental purposes only we ran the flat plate code with local time stepping and the non-reflecting boundary condition using the appropriate Ω and ω_1 for global time stepping schemes. The result is that the convergence behaviour in this case is unexpected. In fact, the convergence is better than with local time stepping with the non-reflecting condition along with it's appropriate Ω and ω_1. The bottom dotted line in (9) shows the convergence behaviour in this case, and another order of magnitude is obtained. Figure (10) shows the pointwise residuals after 5000 iterations in this additional case. Clearly the best steady state is achieved in this way.

This in no way disproves our claim. We obtain better convergence using our non-reflecting boundary condition than with extrapolation conditions both in global and local time stepping regimes. However, it appears that our method of finding the coefficients is not optimal, so that perhaps factors other than long wave disturbances need to be taken into consideration. In any case, the important result that we have demonstrated here is as follows:

Local time stepping schemes converge to steady state faster than global time stepping schemes do because they cause longwave disturbances from
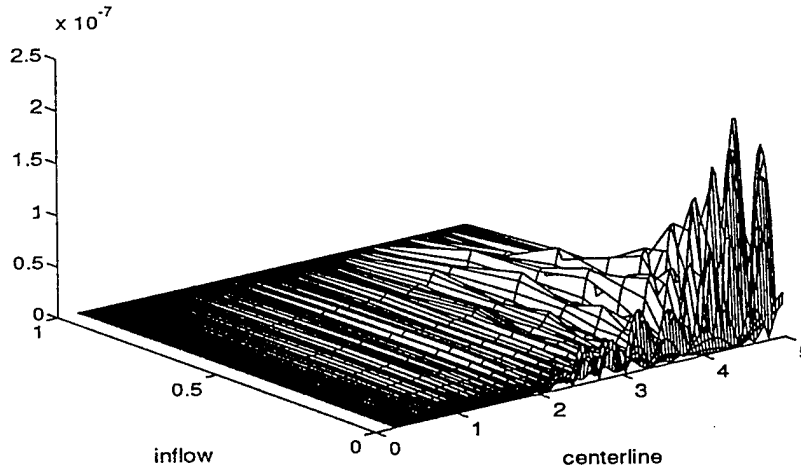
24

Figure 10: Local time stepping run with Ω and ω_1 taking on global time stepping values. Residuals

steady state to decay faster than schemes utilizing global time stepping.

5.3 Compressible Viscous Flow around airfoils

5.3.1 Case 1- Global time stepping without multigrid acceleration

The far-field non-reflecting boundary condition was implemented in the program [9], as a means to test its effectiveness in the compressible viscous subsonic case with $R_l = 5000$ and $M_\infty = 0.5$. An appropriate 257×65 C-mesh was constructed using a hyperbolic grid generator. Often, hyperbolic generators create grids that tend to magnify the intrinsic singularity at the trailing edge. By adding additional control points we have overcome this phenomenon and generated a smooth grid reminiscent of an ellipticly generated one. The outflow boundary was placed 5 chord lengths away from the trailing edge, and was made as perpendicular as possible to the airfoil chord. Two runs were made, one with extrapolation boundary conditions and the other with the nonreflecting boundary condition. In each run, 30000 time steps were taken. Neither multigrid nor other accelerators were used. Minimal artificial viscosity was used to assure convergence. The results that have been obtained are delineated below.

The L^∞ and L^2 norms of the ρ residual are shown in Figures 11 and 12. Clearly the nonreflecting condition accelerates convergence to steady state more than the
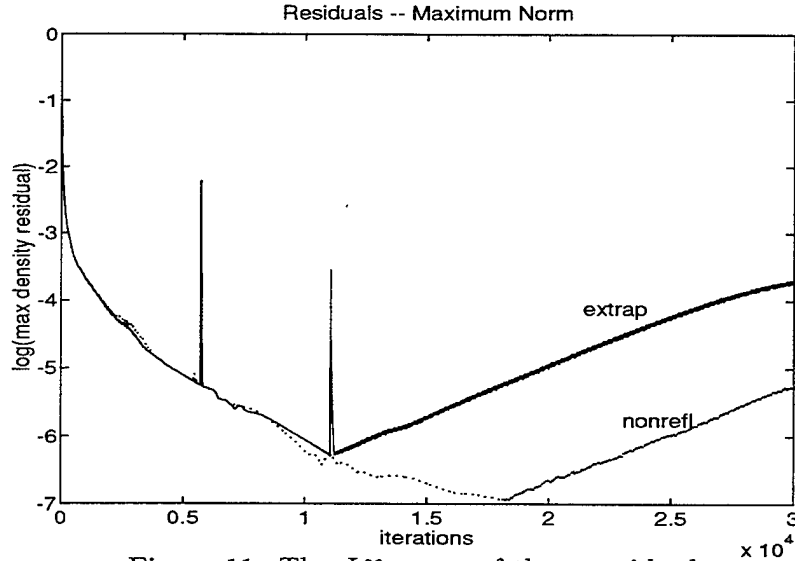
25

Figure 11: The L^∞ norm of the ρ residual

extrapolation condition does. The peaks in the residuals while using extrapolation have not yet been explained. Due to stability considerations (long time numerical integration), in both cases the residuals increase and level off towards the end of the runs, but in the nonreflecting case, the smallest residuals are smaller than in the extrapolation case, and the residuals grow sooner and faster with extrapolation than with the nonreflecting condition. Hence, the nonreflecting condition produces a more robust computational environment, and achieves a better steady state.

In Figures 13 and 14, the pointwise residuals are shown for extrapolation and nonreflecting boundary conditions for 30000 time steps. While 30000 time steps is clearly beyond the optimal computation time, it is still evident that the nonreflecting boundary condition is more effective at reducing residuals than the extrapolation condition. In addition, in Figure 15 the values of ρ and u along the grid line: $j = 5$, $i = 1 - 258$ are shown. This grid line starts in the wake region (far field), then is in the boundary layer (around the airfoil), and returns to the far field. Both conditions give identical results around the airfoil – in the boundary layer. However, in the far field, the nonreflecting condition produces a smoother solution than extrapolating does. While we have shown this result for $j = 5$ only, it is true in the entire wake region.
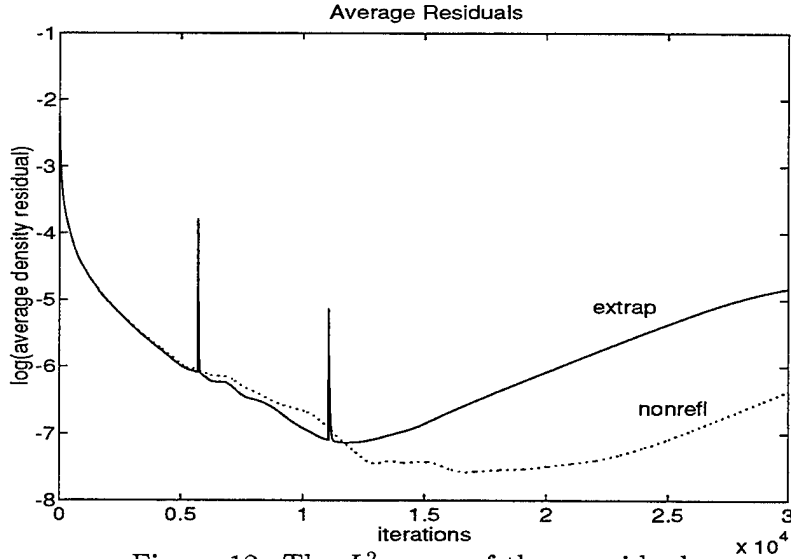
26

Figure 12: The L^2 norm of the ρ residual

5.3.2 Case 2- Global time stepping with multigrid acceleration

In order to decrease the residual further and to stabilize the runs, we have investigated the nonreflecting boundary condition in regimes with global time steps, accelerated to steady state with multigrid techniques.

As we previously mentioned, the nonreflecting boundary condition needs to be modified when using multigrid acceleration in the numerical scheme and it takes the form (4.6).

In this case we compared two runs – one run using multigrid acceleration and extrapolation outflow conditions, and the other run using multigrid acceleration and the above nonreflecting boundary condition. In order to help eliminate short wave disturbances in the y direction, we further introduced the Fourier smoothing as suggested by Ryaben'kii [8]

$$p_{i,j}^n \leftarrow \frac{1}{4}p_{i,j+1}^n + \frac{1}{2}p_{i,j}^n + \frac{1}{4}p_{i,j-1}^n \tag{5.6}$$

locally near the lower and upper corners along the outflow boundary This smoothing transformation was applied each time our nonreflecting boundary condition was called and can be shown to identically kill off the shortest wave in the Fourier expansion.

In the figures which follow (figures 16, 17 and 18), we show the convergence behavior in both the L^∞ and L^2 norms in using at outflow extrapolation and the nonreflecting condition and show residual plots for ρ for both the extrapolation boundary condition and the nonreflecting boundary condition.
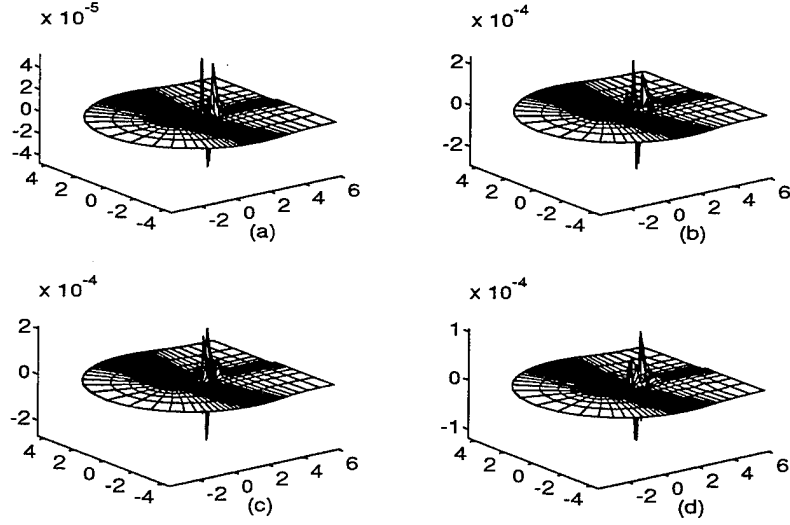
27

Figure 13: Residuals using Extrapolation conditions for (a) ρ, (b) ρu, (c) ρv and (d) e

The same C-grid and other flow parameters were used in these calculations as in the previous subsection. Multigrid acceleration was applied in the following way: 100 W cycles (3 grids) were run first starting on the first coarser grid in order to set up a reasonable initial condition. The results of these sweeps were used as the initial condition for a set of 2000 W cycles (4 grids) starting on the finest grid. Both second order and fourth order artificial viscosity (see [9] and [11]) were applied as well as implicit residual smoothing. Residual smoothing insures that the scheme will converge with a much larger CFL number — hence accelerating convergence.

The results are as follows: The L^2 residual norms obtained using both boundary conditions are nearly identical. However the residual plots indicate that the largest residuals at steady state with the both outflow conditions are at the corners of the outflow boundary (the corner problem) and at inflow, presumably propagated backward from the corners. The maximum norm, L^∞ of the steady state residual while using the nonreflecting boundary condition at outflow, is slightly greater then when using the extrapolation conditions at outflow as is confirmed in figure 16. However, in the wake region, the residuals are smaller when using the nonreflecting boundary condition then when using extrapolation conditions. This is clearly seen in figures 17 and 18.
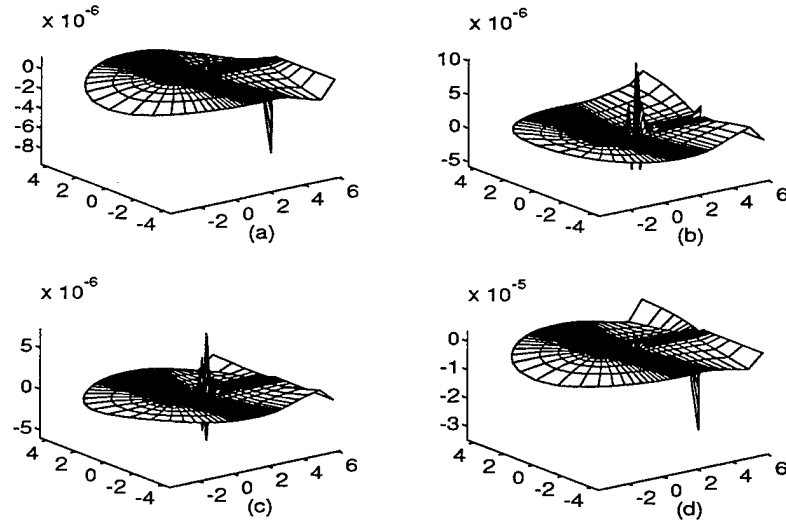
Figure 14: Residuals using Nonreflecting conditions for (a) ρ, (b) ρu, (c) ρv and (d) e

6   Conclusion

We have described the derivation of a nonreflecting far field boundary condition for steady viscous, compressible, two dimensional external flows. This condition produces a smoother far field solution than the presently used extrapolation boundary conditions, while retaining the solution in the boundary layer. It also smooths out the trailing edge singularity by one to two orders of magnitude. The method can be applied to incompressible flows, where it is just as effective in driving residuals down to steady state faster than extrapolation conditions. In addition, nonreflecting boundary conditions of the type described in this work can be developed for schemes whose time stepping is local, as well as for schemes utilizing multigrid acceleration.

In addition to the benefits accrued from using out boundary condition, it is easy to program, and does not require the use of much additional memory in an existing program. Also, its simplicity and local form require little cpu time.

Perhaps the most important feature of our approach is that while in this paper we have chosen to deal with steady state problems, our methodology could be used to develop a condition for evolution equations that do not reach a steady state. In this case, we would perturb the linerized equations about the appropriate wave group that we wish to absorb (not necessarily about long waves) and proceed exactly as we did for steady state flows. Of course an appropriate far field profile needs to be formulated as well for each flow, which now may be time dependent. Hence our methodolgy is
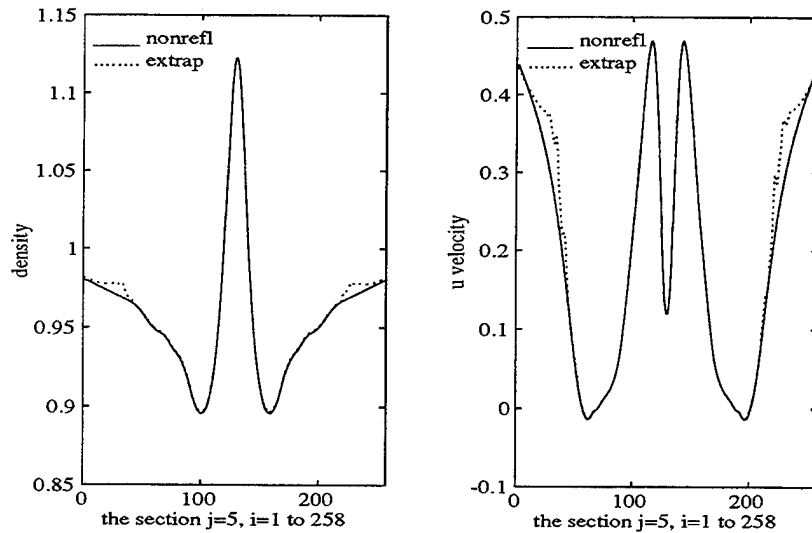
29

Figure 15: The values of ρ and u along the grid line: $j = 5$, $i = 1 - 258$

versatile and is shown to be effective in reducing residuals in external viscous flows.

References

[1] S. Abarbanel, A. Bayliss and L. Lustman, *Non-reflecting Boundary Conditions for the Compressible Navier-Stokes Equations*, Proc. of the 7th International Congress in Computing Methods in Applied Science and Engineering, North Holland, (1986).

[2] S. Abarbanel, A. J. Kumar, *Compact High Order Schemes for the Euler Equations*, J. Scientific Computing, Vol. 3, (1988), 275-288.

[3] G. K. Batchelor, *An Introduction to Fluid Dynamics*, Cambridge University Press, (1967).

[4] G. Birkhoff, G.-Carlo Rota, *Ordinary Differential Equations 4th ed.*, Wiley, (1989).

[5] B. Gustaffson, H.-O. Kreiss, *Boundary Conditions for Time Dependent Problems with an Artificial Boundary*, J. Comp. Phys., Vol. 30, (1979), 333-351.

[6] A. Jameson, H. Schmidt, and E. Turkel, *Numerical Solutions of the Euler Equations by Finite Volume Methods Using Runge-Kutta Time-Stepping Schemes*, AIAA Paper No.81-1258, (1981)
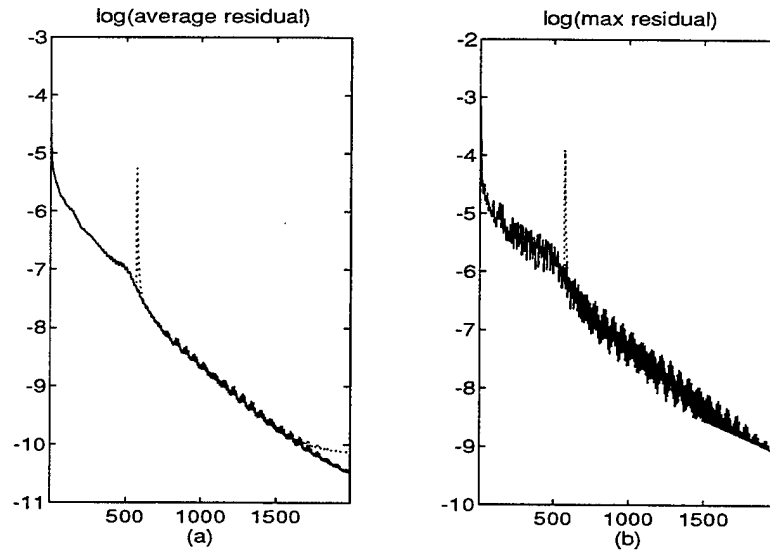
30

Figure 16: The L^2, (a), and L^∞,(b) norms of the ρ residual after 2000 multigrid W cycles. Legend: $\cdots$ - nonreflecting conditions, — - extrapolation conditions

[7] R.D. Richtmeyer, K.W. Morton, *Difference Methods for Initial Value Problems, 2nd ed.*, Interscience, (1967).

[8] Private Communication.

[9] R. C. Swanson, E. Turkel, *Artificial Dissipation and Central Difference Schemes for the Euler and Navier-Stokes Equations*, AIAA CFD Conference, AIAA paper No. 87-1107-cp, (1987).

[10] E. Turkel, *Numerical Methods for Large-Scale, Time-Dependent Paritial Differential Equations*, Computational FLuid Dynamics Vol 2, W. Kollmann ed., Hemisphere Publication Co., (1980), 127-262.

[11] E. Turkel, *Improving the Accuracy of Central Difference Schemes*, 11th International Conference on Numerical Methods in Fluid Dynamics, Springer-Verlag Lecture Notes in Physics, Vol 323, (1988), 586-591.
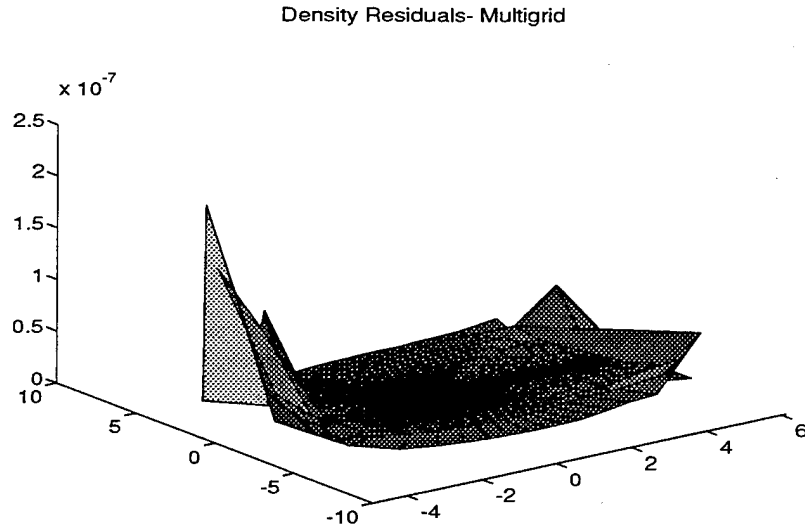
[12] Private Communication.

Figure 17: The ρ residuals after 2000 multigrid W cycles. Extrapolation outflow conditions.
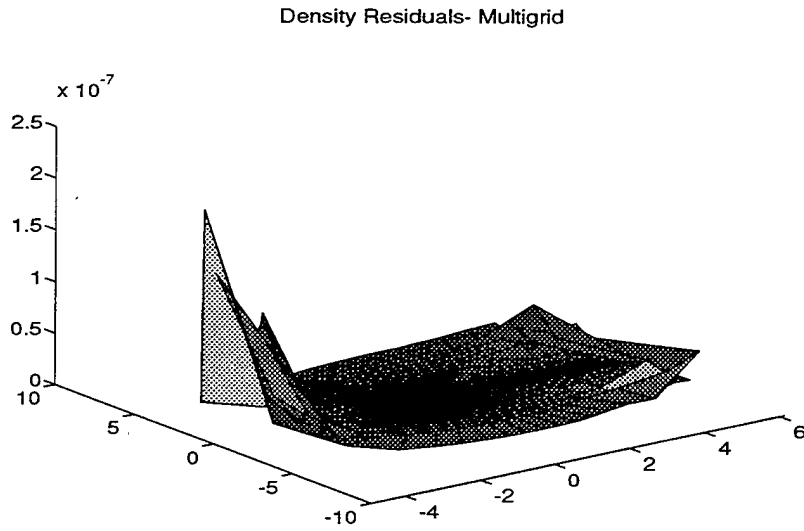

Figure 18: The ρ residuals after 2000 multigrid W cycles. Nonreflecting outflow conditions.

32

REPORT DOCUMENTATION PAGE

Public reporting burden for this collection of information is estimated to average 1 hour per response, including the time for reviewing instructions, searching existing data sources, gathering and maintaining the data needed, and completing and reviewing the collection of information. Send comments regarding this burden estimate or any other aspect of this collection of information, including suggestions for reducing this burden, to Washington Headquarters Services, Directorate for Information Operations and Reports, 1215 Jefferson Davis Highway, Suite 1204, Arlington, VA 22202-4302, and to the Office of Management and Budget, Paperwork Reduction Project (0704-0188), Washington, DC 20503.

1. AGENCY USE ONLY *(Leave blank)*	2. REPORT DATE September 1995	3. REPORT TYPE AND DATES COVERED Contractor Report

4. TITLE AND SUBTITLE
A FAR-FIELD NON-REFLECTING BOUNDARY CONDITION FOR TWO-DIMENSIONAL WAKE FLOWS

5. FUNDING NUMBERS
C NAS1-19480
WU 505-90-52-01

6. AUTHOR(S)
Jeffrey S. Danowitz
Saul A. Abarbanel
Eli Turkel

7. PERFORMING ORGANIZATION NAME(S) AND ADDRESS(ES)
Institute for Computer Applications in Science
and Engineering
Mail Stop 132C, NASA Langley Research Center
Hampton, VA 23681-0001

8. PERFORMING ORGANIZATION REPORT NUMBER
ICASE Report No. 95-63

9. SPONSORING/MONITORING AGENCY NAME(S) AND ADDRESS(ES)
National Aeronautics and Space Administration
Langley Research Center
Hampton, VA 23681-0001

10. SPONSORING/MONITORING AGENCY REPORT NUMBER
NASA CR-198214
ICASE Report No. 95-63

11. SUPPLEMENTARY NOTES
Langley Technical Monitor: Dennis M. Bushnell
Final Report
Submitted to Journal of Computational Physics

12a. DISTRIBUTION/AVAILABILITY STATEMENT
Unclassified–Unlimited

Subject Category 64

12b. DISTRIBUTION CODE

13. ABSTRACT *(Maximum 200 words)*

Far-field boundary conditions for external flow problems have been developed based upon long-wave perturbations of linearized flow equations about a steady state far field solution. The boundary improves convergence to steady state in single-grid temporal integration schemes using both regular-time-stepping and local-time-stepping. The far-field boundary may be near the trailing edge of the body which significantly reduces the number of grid points, and therefore the computational time, in the numerical calculation. In addition the solution produced is smoother in the far-field than when using extrapolation conditions. The boundary condition maintains the convergence rate to steady state in schemes utilizing multigrid acceleration.

14. SUBJECT TERMS
far-field boundary conditions; viscous flows; non-reflecting boundary conditions; computational fluid dynamics

15. NUMBER OF PAGES
34

16. PRICE CODE
A03

17. SECURITY CLASSIFICATION OF REPORT Unclassified	18. SECURITY CLASSIFICATION OF THIS PAGE Unclassified	19. SECURITY CLASSIFICATION OF ABSTRACT	20. LIMITATION OF ABSTRACT

NSN 7540-01-280-5500